

Changes in Community Structure of Brain Dynamic Functional Connectivity States in Mild Cognitive Impairment

Hongwei Wang,^a Zhihao Zhu,^b Hui Bi,^a Zhongyi Jiang,^a Yin Cao,^c Suhong Wang^d and Ling Zou^{b,e,*}

^a School of Computer Science and Artificial Intelligence, Aliyun School of Big Data, School of Software, Changzhou University, Changzhou, Jiangsu 213164, China

^b School of Microelectronics and Control Engineering, Changzhou University, Changzhou, Jiangsu 213164, China

^c The Affiliated Changzhou Second People's Hospital of Nanjing Medical University, Changzhou, Jiangsu 213164, China

^d Clinical Psychology, The Third Affiliated Hospital of Soochow University, Juqian Road No. 185, Changzhou, Jiangsu 213164, China

^e The Key Laboratory of Brain Machine Collaborative Intelligence Foundation of Zhejiang Province, Hangzhou, Zhejiang 310018, China

Abstract—Recent researches have noted many changes of short-term dynamic modalities in mild cognitive impairment (MCI) patients' brain functional networks. In this study, the dynamic functional brain networks of 82 MCI patients and 85 individuals in the normal control (NC) group were constructed using the sliding window method and Pearson correlation. The window size was determined using single-scale time-dependent (SSTD) method. Subsequently, k-means was applied to cluster all window samples, identifying three dynamic functional connectivity (DFC) states. Collective sparse symmetric non-negative matrix factorization (cssNMF) was then used to perform community detection on these states and quantify differences in brain regions. Finally, metrics such as within-community connectivity strength, community strength, and node diversity were calculated for further analysis. The results indicated high similarity between the two groups in state 2, with no significant differences in optimal community quantity and functional segregation ($p < 0.05$). However, for state 1 and state 3, the optimal community quantity was smaller in MCI patients compared to the NC group. In state 1, MCI patients had lower within-community connectivity strength and overall strength than the NC group, whereas state 3 showed results opposite to state 1. Brain regions with statistical difference included MFG.L, ORBinf.R, STG.R, IFGtriang.L, CUN.L, CUN.R, LING.R, SOG.L, and PCUN.R. This study on DFC states explores changes in the brain functional networks of patients with MCI from the perspective of alterations in the community structures of DFC states. The findings could provide new insights into the pathological changes in the brains of MCI patients. © 2024 IBRO. Published by Elsevier Inc. All rights reserved.

Key words: MCI, fMRI, dynamic functional connectivity, community structures.

INTRODUCTION

Mild Cognitive Impairment (MCI) manifests as cognitive impairments that do not meet the diagnostic criteria for Alzheimer's disease (AD), nor significantly affect patients' intellectual functioning or daily activities. It is widely considered as a precursor stage of AD (Liu et al.,

2022). Timely and effective intervention is crucial for improving treatment outcomes and delaying disease progression in MCI patients. Therefore, it is critical to analyze and accurately identify brain characteristics of MCI patients.

Resting-state functional magnetic resonance imaging (rs-fMRI) boasts some advantages such as non-invasiveness, high spatial resolution, stable and reliable results, and a straightforward experimental procedure (Fathi et al., 2022). It has improved our understanding of brain functional organization and human brain changes following disease and injury. Various studies have captured changes in the brains of MCI and AD patients in terms of regions, functions, and overall brain connectivity (van den Heuvel & Hulshoff Pol, 2010). For example, Wang et al. (Wang et al., 2012) discovered reduced functional connectivity in regions such as the left thalamus and

*Correspondence to: L. Zou, School of Microelectronics and Control Engineering, Changzhou University, Changzhou, Jiangsu 213164, China.

E-mail address: zouling@cczu.edu.cn (L. Zou).

Abbreviations: 2dPCA, two-dimensional principal component analysis; cssNMF, Collective sparse symmetric non-negative matrix factorization; DFC, dynamic functional connectivity; MCI, Mild Cognitive Impairment; NC, normal control; rs-fMRI, Resting-state functional magnetic resonance imaging; SSE, sum of squared errors; SSTD window-sizes, single-scale time-dependent window-sizes.

a set of regions in MCI patients such as bilateral cuneus, middle occipital gyrus (MOG), superior frontal gyrus (SFG). They observed reduced connectivity in the right thalamus and some regions, such as bilateral cuneus, MOG, fusiform gyrus (FG). They also observed that functional connectivity between the left and right thalamus increased. In recent years, many researchers studying common neurological disorders and diseases have directed their attention towards dynamic functional connectivity (DFC) (Du et al., 2021; Zhang et al., 2021; Gao et al., 2022; Wei et al., 2022; Xu et al., 2023). Jiao et al. (Jiao et al., 2021) identified differences in DFC between early MCI (eMCI), late MCI (lMCI), and normal control (NC) by comparing repetitive patterns during rest or task states. Their graph theory metrics revealed states of both integration and segregation of functional connectivity. Changes in short-term dynamic modalities have also been found in diseases like autism spectrum disorder (ASD), attention-deficit/hyperactivity disorder (ADHD), bipolar disorder (BD) II depression (Chen et al., 2022; Gao et al., 2022; Zhu et al., 2023). In DFC studies, it is common to generate a set of FC matrices for each subject by calculating sliding window correlations (Hindriks et al., 2016; Ma et al., 2021; Gao et al., 2022; Spencer & Goodfellow, 2022). However, choosing an appropriate window size is a critical issue. Zhuang et al. (Zhuang et al., 2020) proposed the use of SSTD to determine the window size for DFC, a data-driven approach.

In the study of brain functional networks, community structure is one of the most important topological features. Brain functional networks, like real-world complex networks, exhibit overlapping community structures (Najafi et al., 2016), meaning that a node can serve multiple functions and participate in multiple communities in the brain's actual functioning. Due to compensatory mechanisms triggered by damage in certain brain regions of MCI patients, alterations in their brain functional networks have occurred (Prieto del Val et al., 2018). Some research held that features related to community structure are valuable for detecting neurological disorders and diseases. Changes in overlapping community structures have been identified in diseases such as Alzheimer's disease (AD), Major Depressive Disorder (MDD), and juvenile myoclonic epilepsy (JME) (Chen et al., 2021; Han et al., 2022; Vataman et al., 2023). However, previous studies mainly used static functional connectivity for community detection, and few investigations explore changes in community structure from the perspective of DFC states.

This study combines the sliding window and k-means to identify repetitive modalities in MCI and NC subjects, and employs collective sparse symmetric non-negative matrix factorization (cssNMF) (Li et al., 2018) to detect overlapping community structures. The study also explores changes in the community structure of different DFC states in MCI patients from the perspective of alterations in DFC state community structures and functional network segregation. Additionally, this study aims to identify different nodes that repeatedly appear in the research.

EXPERIMENTAL PROCEDURES

Data acquisition and preprocessing

In this study, the fMRI data of the NC group and the MCI subjects were obtained from the Alzheimer's Disease Neuroimaging Initiative (ADNI) database (<https://adni.loni.usc.edu/>). It is a multicenter longitudinal study aiming primarily to detect biomarkers for clinical use and to test whether the progression of MCI and the early stages of AD can be measured by combining continuous MRI, PET, other biomarkers, clinical, and neuropsychological assessments.

The study analyzed fMRI data from 167 participants, including 82 individuals with MCI (44 females, 38 males, average age 73.55) and 85 individuals in the NC group (43 females, 42 males, average age 72.76). fMRI data were acquired using various models of 3 T Siemens medical systems. The scanning parameters used during the acquisition process were as follows: repeat time (TR) = 3000.0 ms, echo time (TE) = 30.0 ms, flip angle = 90.0°, matrix X = 448.0 pixels, matrix Y = 448.0 pixels, pixel spacing X = 3.4 mm, pixel spacing Y = 3.4 mm, slice thickness = 3.4 mm, pulse sequence = EP, slices = 197.0, and slice number = 48.

Resting-state fMRI data preprocessing was conducted using the DPARSF (Chao-Gan & Yu-Feng, 2010) (<http://www.rfmri.org/>), SPM12 (<http://www.fil.ion.ucl.ac.uk/spm/>), and MATLAB. During preprocessing, all subjects underwent slice timing correction, head motion correction, co-registration, normalization, and filtering. To mitigate the effects of gradient magnetic field instability, the first 10 time points of the data were discarded. Data from subjects with excessive head motion (translation > 3.0 mm, rotation > 3.0°) were excluded. Only data meeting the criteria were used.

During co-registration, the images were normalized to standard MNI space using an EPI template, resampled to $3 \times 3 \times 3 \text{ mm}^3$ voxels, and smoothed using a 6 mm full-width at half-maximum Gaussian kernel. Subsequently, linear detrending and bandpass filtering (0.01–0.08 Hz) were applied to the images to suppress low-frequency drift and physiological noise. The entire brain was divided into 90 regions of interest (ROIs) using the Automated Anatomical Labeling (AAL) template, and the average time series of all voxels were extracted for each ROI.

Calculation of DFC and identification of repetitive states

When calculating DFC, we computed the single-scale time-dependent (SSTD) window size for the sliding window approach (Zhuang et al., 2020). The SSTD window size is time-dependent and data-driven, based on the frequency content at each time point of the time series, and is calculated without any prior information. The dynamic FC matrix computed using the SSTD window size captures more temporal dynamic information related to behavior and cognitive functions. Subsequently, the sliding window method and Pearson correlation coefficient

cient method were used to calculate the DFC, with a window size equal to the calculated SSTD window size. After each calculation, the window was slid back one time point.

To identify repetitive patterns in DFC, K-means clustering analysis was applied to all samples. Before performing clustering analysis, a Fisher-Z transformation was applied to the correlation matrices to enhance their normality. The data was also dimensionally reduced using two-dimensional principal component analysis (2dpca), and the remaining information after dimensionality reduction was evaluated by calculating cumulative scores. We set the cumulative score threshold to 0.90, aiming to retain at least 90% of the original data variance.

To mitigate the impact of data redundancy on the computation time and results of clustering, a second-level subsampling of the participant's sliding windows was performed (Allen et al., 2014). The subsampling criteria involved selecting 8–12 windows with local maximum variance from the 187 windows of each participant, resulting in an average of 10 windows per participant as initial clustering samples.

Since the samples were high-dimensional data, the L1 distance function (Manhattan distance) was chosen over the L2 distance function (Euclidean distance) as a more effective similarity measure (Allen et al., 2014). The randomization of initial centroids for K-means was repeated 500 times, with a maximum of 1000 iterations, to avoid local minima. The value of K was iterated over from 2 to 10 with a step size of 1. The squared distance error between the centroids of each cluster and the sampling

points of the cluster, known as the sum of squared errors (SSE) or distortion, was computed for each cluster, and the elbow criterion was used to determine the optimal number of clusters.

Once the optimal value of K was determined, K-means clustering was performed using K as the number of clusters and the results of the second-level subsampling as the cluster centers, resulting in K distinct repetitive modes for the two groups of participants.

The detailed steps of this study are shown in Fig. 1.

Detection of overlapping community structures

In the actual operation of the brain, a specific brain region can fulfill multiple functions, demonstrating its ability to engage in various communities and contribute to the formation of an overlapping community structure. Therefore, cssNMF (Li et al., 2018) was applied to conduct overlapping community detection across all modalities of two groups of participants. Before the analysis, we computed the average of all DFC values attributed to a particular modality for each participant, retaining only the node-to-node connections with functional connectivity strengths ranking within the top 10%. cssNMF inherently captures inter-subject variability in community strength without necessitating additional post-processing steps. It enables the direct interpretation-based identification of highly replicable group-level community structures. The objective function of cssNMF is as follows:

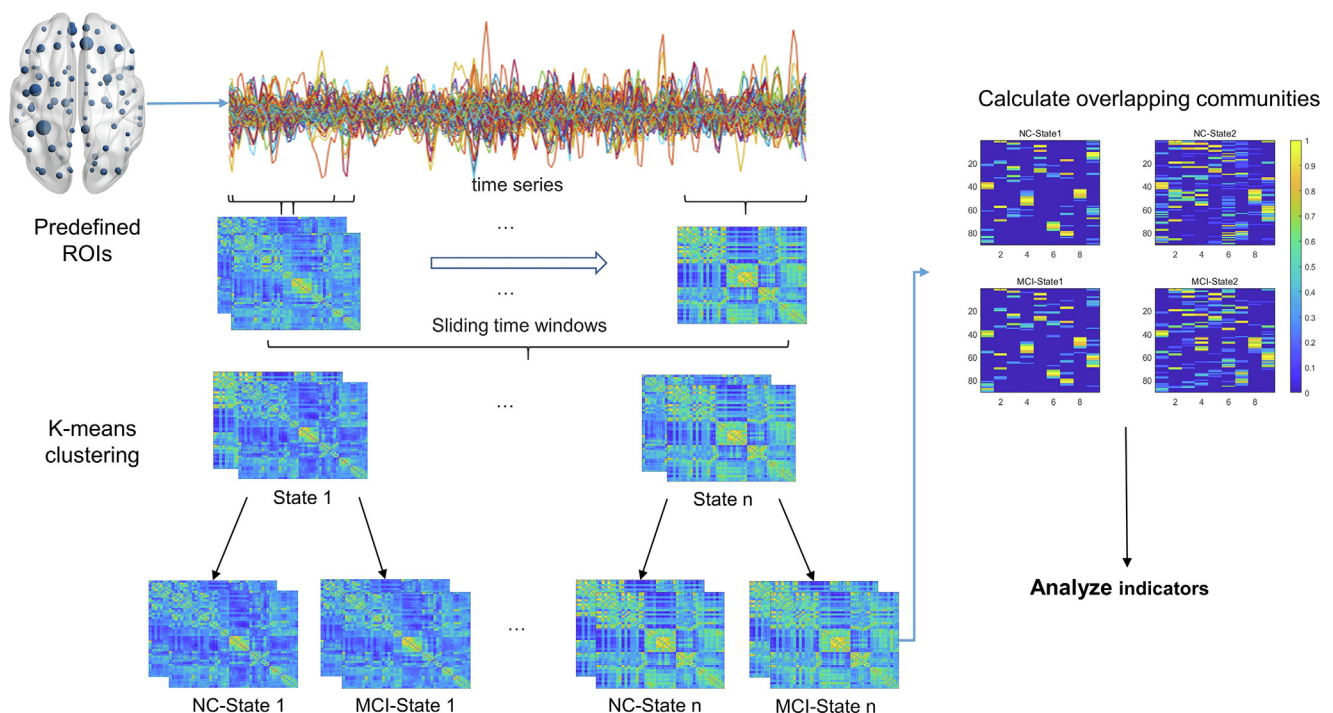


Fig. 1. Overview of DFC analysis in this study. It includes the following steps: (a) Extraction of time series based on the AAL template and construction of brain functional networks using a sliding window approach; (b) Clustering using the k-means method; (c) Overlapping community detection for three states, followed by statistical and metric analysis.

$$\begin{aligned} \min_{H, S \geq 0} \frac{1}{2} \sum_{i=1}^M \|G^i - HS^iH^T\|_F^2 + \beta \|H\|_1 \\ \text{s.t. } \forall j: \max(h_j) = 1, j = 1, \dots, k \end{aligned} \quad (1)$$

Where $H(H = (h_1, \dots, h_k) \in \mathbb{R}^{n \times k})$ represents the detected results of overlapping community detection, k is the predetermined number of communities used for community detection with the cssNMF model, h_j represents the j -th community. Where $G^i (G^i \in \mathbb{R}^{n \times n} (i = 1, 2, \dots, M))$ is the symmetric non-negative correlation matrix of participants, M represents the number of participants. For each correlation matrix, specific information is retained individually in $S^i (S^i = (s_1^i, \dots, s_k^i) \in \mathbb{R}^k)$, s_j^i represents the strength of the j -th community of the i -th correlation matrix. Where $\beta (\beta > 0)$ is the regularization parameter used to control the level of sparsity in the obtained communities, ensuring that only the most relevant nodes are retained within the communities.

The parameters k and β are determined through a grid search with a dual cross-validation process. The testing error is defined as follows:

$$\text{Test error} = \frac{\sum_{i=1}^{N_{\text{test}}} \|G_{\text{test}}^i - H_{\text{train}} S_{\text{test}}^i H_{\text{train}}^T\|_F^2}{\sum_{i=1}^{N_{\text{test}}} \|G_{\text{test}}^i \bar{G}_{\text{test}}\|_F^2} \quad (2)$$

Due to random initialization and non-convex constraints, cssNMF needs to be run multiple times. Thus, for each computation in the experiment, the cssNMF algorithm was executed 20 times, and the minimum value of the objective function was selected for subsequent analysis.

Upon obtaining the overlapping community results for all modalities of the two participant groups, the top 10 brain regions with significant differences in weight values within each community for both groups were separately recorded. Additionally, the distinct nodes that contributed to multiple functions in the community detection of both groups were identified.

Functional segregation and node functional diversity

In this study, functional segregation is characterized using the within-community connection strength and the overall community strength (Han et al., 2022). For each participant, the weights of within-community connections are utilized to represent the within-community connection strength:

$$\sum_{p=1}^k \|s_p^j h_p h_p^T\|_1 \quad (3)$$

For each participant, the overall community strength is represented as the sum of all community strengths (s_p^j):

$$\sum_{p=1}^k s_p^j \quad (4)$$

After obtaining the overlapping community structures and participant-specific results, the method for characterizing functional diversity of the j -th node for a specific participant i is as follows (Han et al., 2022):

$$-\sum_{p=1}^k P_{jp}^i \ln P_{jp}^i \quad (5)$$

RESULTS

K-means clustering analysis

In determining the optimal number of clusters, we calculated the SSE and used the elbow criterion to identify the optimal number of clusters as 3, as shown in Fig. 2.

As the number of clusters K increases, the SSE decreases. However, when the number of clusters reaches a certain point, the centers of each group no longer significantly approach their respective internal data points. At this point, increasing the number of clusters no longer significantly reduces clustering error. The improvement in performance becomes markedly smaller when K reaches 3.

The following are the repetitive patterns identified with K set to 3. In the NC group, the three states respectively account for 46.04%, 42.90%, and 11.05% of the sliding windows, while in the MCI group, they account for 34.76%, 47.85%, and 17.39%, respectively. Notably, state 3 has a relatively low proportion in both groups (see Fig. 3).

Overlapping community detection and analysis

Parameter selection. The results of dual cross-validation for selecting the optimal number of communities k , and the sparsity coefficient β , are depicted in the following figure. The influence of β on testing error remains relatively consistent when it varies between 0 and 1. For all groups, the testing error decreases as k increases, with minimal changes in testing error beyond $k = 12$. For each state, in state 1, the testing error for both the NC and MCI groups decreases slightly after $k = 10$ and $k = 8$ respectively. In state 2, the testing error for both groups demonstrates a smooth variation. In state 3, the testing error for the NC and MCI groups decreases slightly after

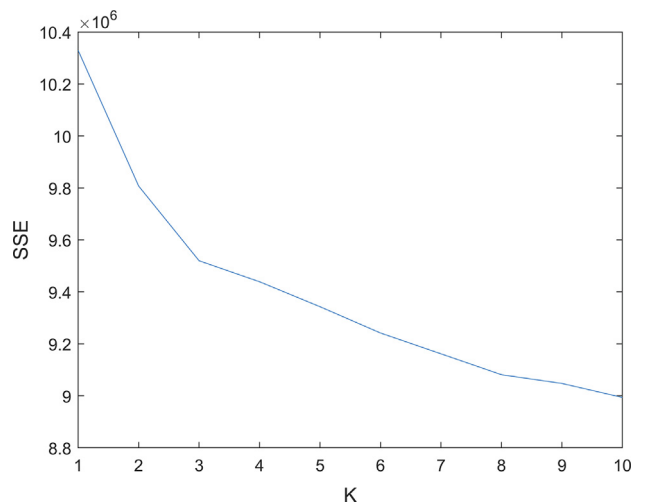


Fig. 2. Variation of sum of squared errors (SSE) across different numbers of clusters (K).

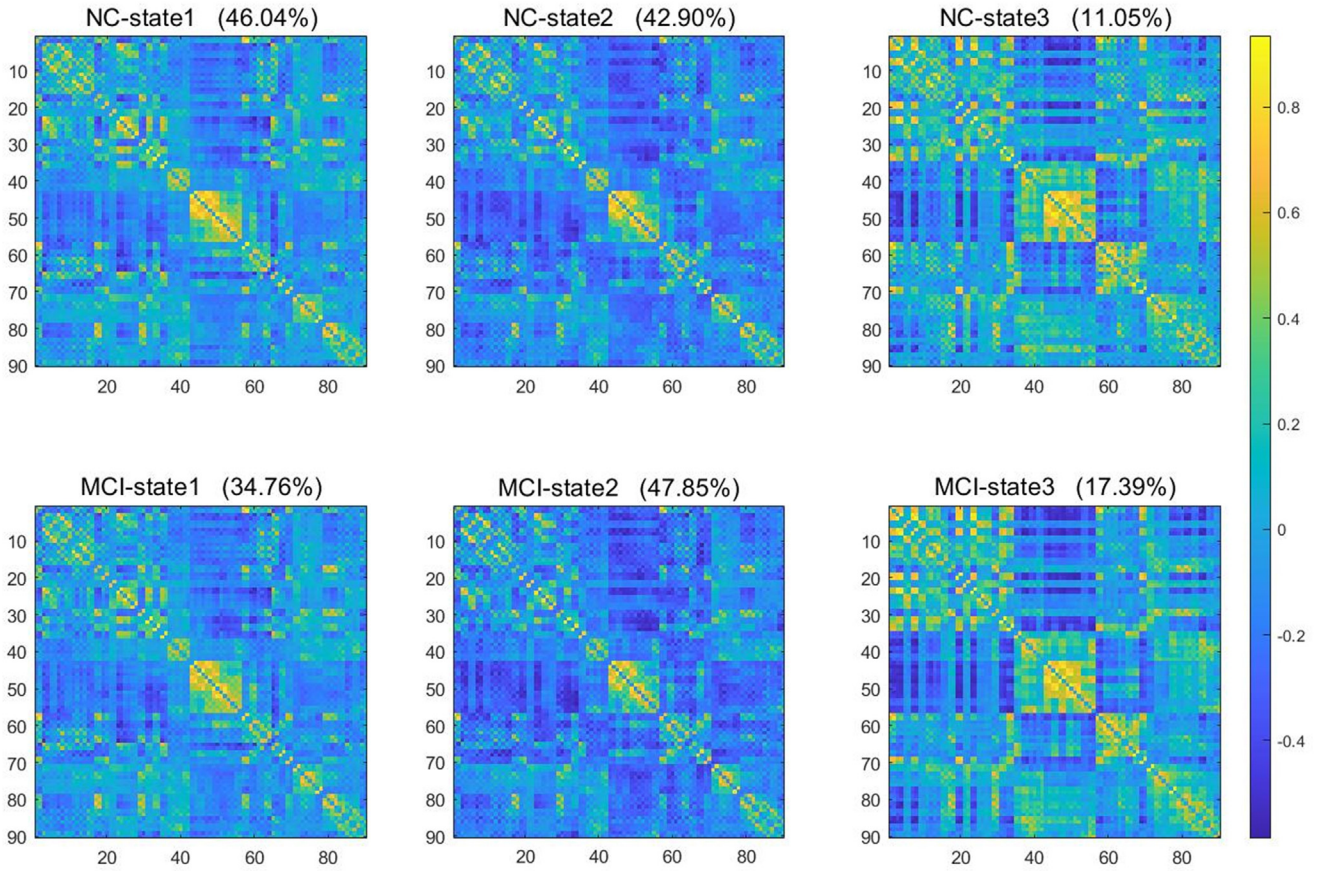


Fig. 3. Functional connectivity matrices composed of the average values from the NC group and the MCI group after clustering into three states.

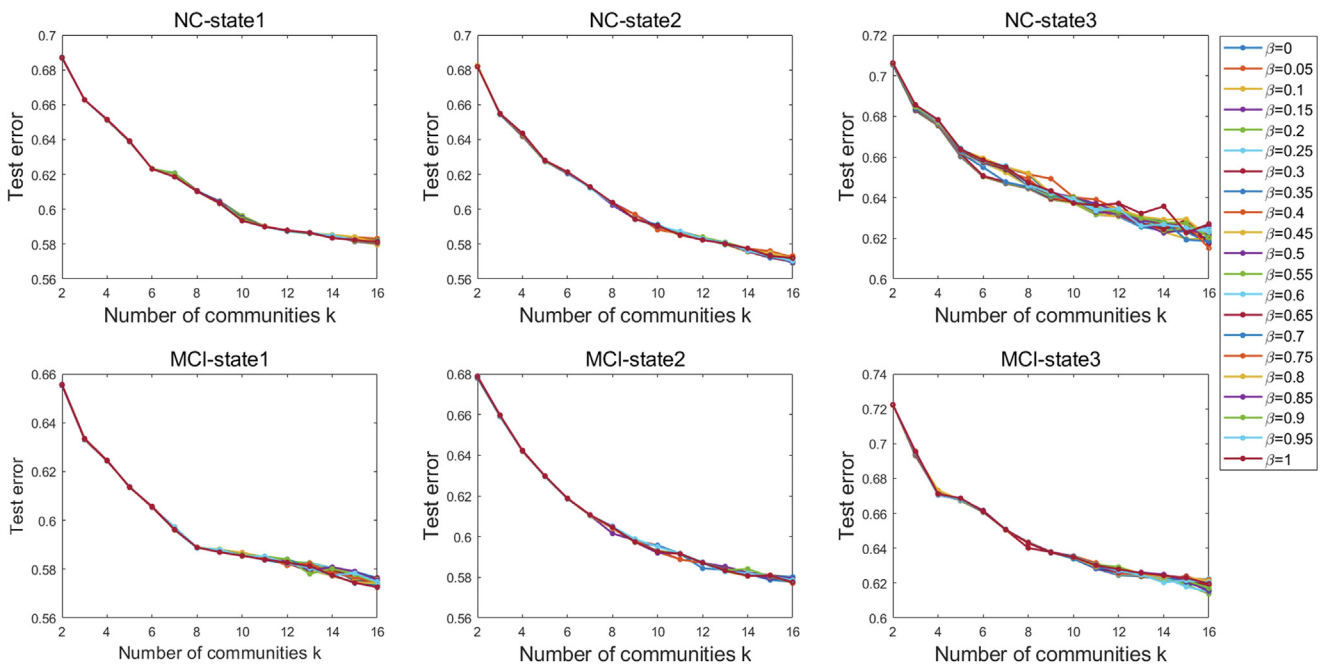


Fig. 4. Parameter selection for cssNMF through dual cross-validation.

$k = 6$ and $k = 8$ respectively, with a sharp reduction in changes in error magnitude after $k = 5$ and $k = 4$.

Taking all factors into consideration, subsequent research on the three states was conducted in two rounds of experiments, with parameter settings of $\beta = 0.1$, $k = 8$ for one round and $\beta = 0.1$, $k = 12$ for the other round.

The upper and lower rows respectively display the testing error results for the three states of the NC group and the MCI group (see Fig. 4).

Overlapping community differences. Figs. 5 and 6 represent the results of overlapping community detection for the NC and MCI group data for two modalities, respectively, using input parameters of $\beta = 0.1$, $k = 8$, and $\beta = 0.1$, $k = 12$. In both sets of experiments, the differences in community detection between the two groups in state 1 are primarily concentrated within fewer communities. The results for community detection in state 2 are quite similar between the two groups, while the differences in the results of community detection are more pronounced in state 3.

When $k = 8$, it was found that in state 1, the differences between the community detections of the two groups are primarily concentrated in communities 1 and 2. While in state 2, the differences are minimal, only showing slight variations in brain regions with lower community weights. In state 3, the differences are mainly focused on the 6th, 7th, and 8th communities. However, compared to state 1 and state 2, the differences between various communities are more significant. Apart from the mentioned communities, there are minimal changes in other communities for the MCI patients (see Fig. 5).

When $k = 12$, it was found that in state 1, the differences between the community detections of the

two groups are primarily concentrated in the 8th and 11th communities. In state 2, the differences are mostly present in nodes with lower community weights, with a significant difference in the twelfth community. In state 3, the differences are significant in the 2nd, 4th, 5th, 7th, and 12th communities. Compared to state 1 and state 2, the differences between various communities are more pronounced. Apart from the mentioned communities, there are minimal changes in other communities for the MCI patients (see Fig. 6).

From a comparative perspective on various communities, we conducted statistical analyses on nodes with significant differences in both $k = 8$ and $k = 12$ conditions, retrieving their corresponding Resting State Networks (RSNs) (He et al., 2009). For state 1 and state 2, we identified the top 10 brain regions with the largest differences in values. Given the higher number of brain regions with differences in state 3, we performed statistical analyses on brain regions with weight differences exceeding 0.5 (see Fig. 7):

For State 1, nodes with substantial differences include PreCG.R, SPG.R, STG.R (Sensorimotor), ACG.R (Default mode), MFG.L, IPL.R (Attention), HIP.L, CAU.L, PUT.R, TPOmid.R (Subcortical).

For State 2, nodes with substantial differences include SFGdor.R, SFGmed.R (Sensorimotor), MFG.L, IFGoperc.L, IFGtriang.L, ORBinf.R, ITG.L (Attention), LING.L, LING.R (Visual), TPOmid.L (Subcortical).

For State 3, nodes with substantial differences include INS.R, PoCG.L, PoCG.R, SPG.L, PCL.L, PCL.R, STG.R (Sensorimotor), SFGmed.L, PCG.L, PCG.R, PCUN.R, MTG.R (Default mode), IFGoperc.R, IFGtriang.R, ORBinf.R (Attention), CUN.L, CUN.R, SOG.L, SOG.R, MOG.L, MOG.R (Visual), OLF.R (Subcortical).

Notably recurring nodes include MFG.L and ORBinf.R (Attention), as well as STG.R (Sensorimotor).

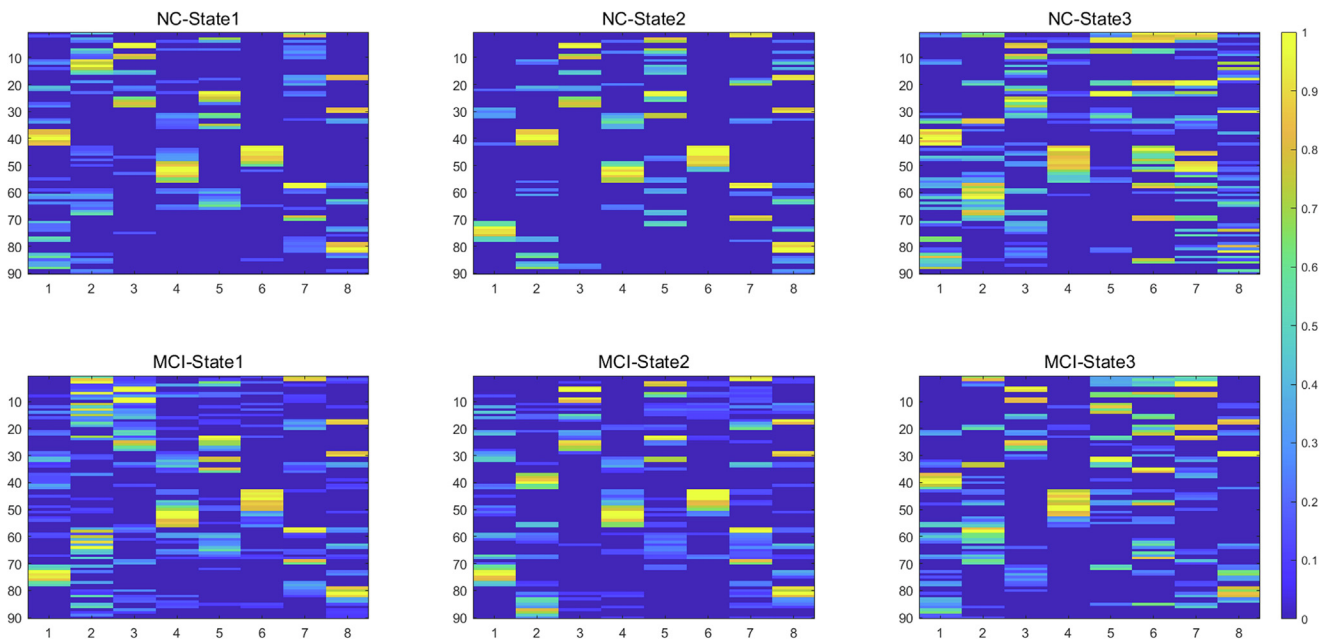


Fig. 5. Overlapping community detection results with $k = 8$ and $\beta = 0.1$.

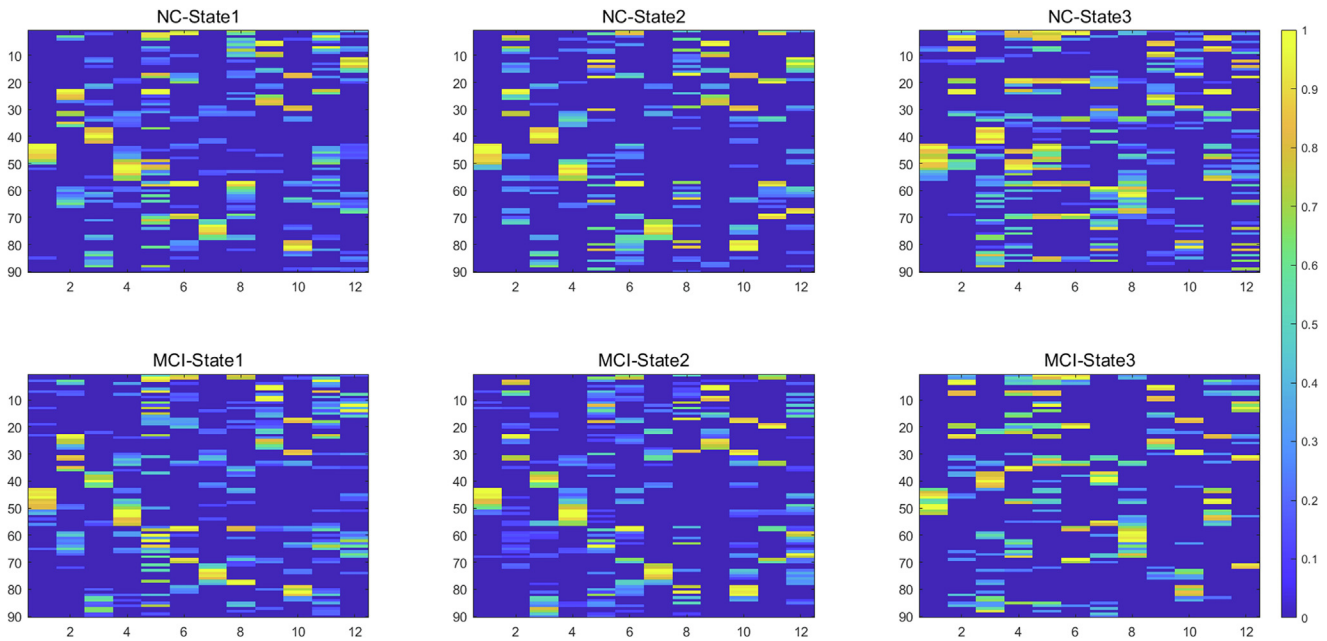


Fig. 6. Overlapping community detection results with $k = 12$ and $\beta = 0.1$.

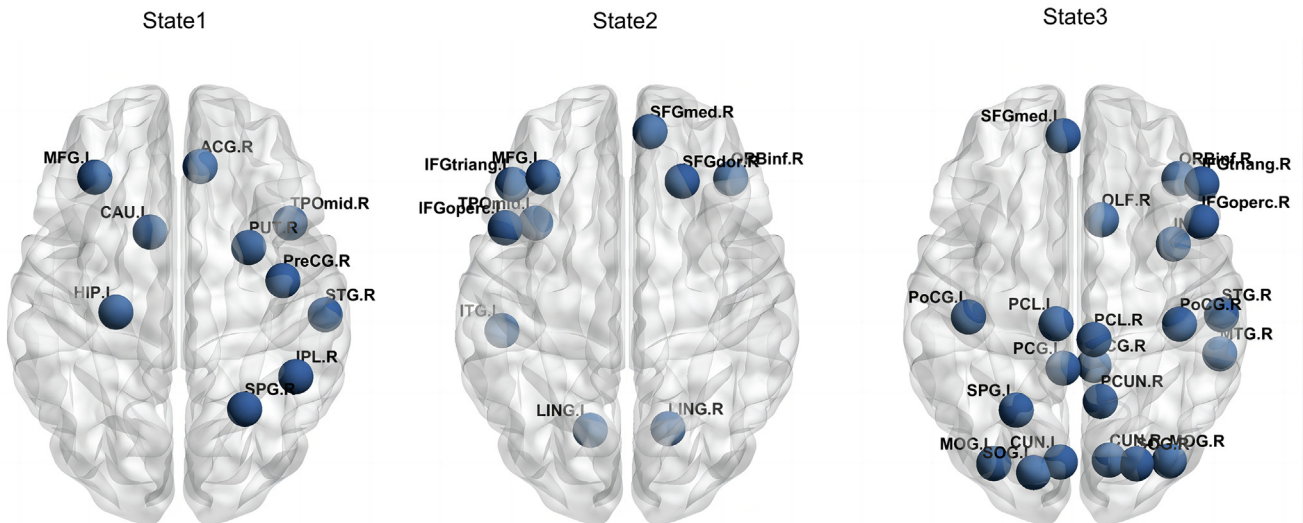


Fig. 7. Nodes with significant differences in various communities for $k = 8$ and $k = 12$ conditions.

From the perspective of overlapping nodes in various communities, we conducted statistical analyses on nodes that exhibited differences in both the $k = 8$ and $k = 12$ experiments, and retrieved their corresponding Resting State Networks (RSNs) (see Fig. 8):

For State 1, differing nodes include SMA.R (Sensorimotor), AMYG.L, TPomid.L (Subcortical), FFG.R (Visual), PCUN.L, PCUN.R (Default mode). All these nodes provide multiple functions in the NC group but not in the MCI group.

For State 2, differing nodes include MFG.L (Attention), SFGmed.L, PCG.L, ITG.R (Default mode). SFGmed.L and PCG.L have conflicting results between the two detections, while the rest provide multiple functions in the NC group but not in the MCI group.

For State 3, differing nodes include ORBsup.L, ORBmid.L, ORBmid.R, ANG.L (Attention), ORBsupmed.R, PCG.R (Default mode), INS.L (Sensorimotor), PHG.L, PAL.L, THA.R (Subcortical), SOG.L (Visual). PCG.R has conflicting results between the two detections, while ORBsupmed.R, PHG.L, PAL.L provide multiple functions in the NC group but not in the MCI group, and others exhibit the opposite pattern.

Notably, there are no nodes that consistently appear in the differences among nodes providing multiple functions across the three states.

Functional segregation. Functional segregation of the community structure is evaluated based on the within-community connectivity strength and the overall

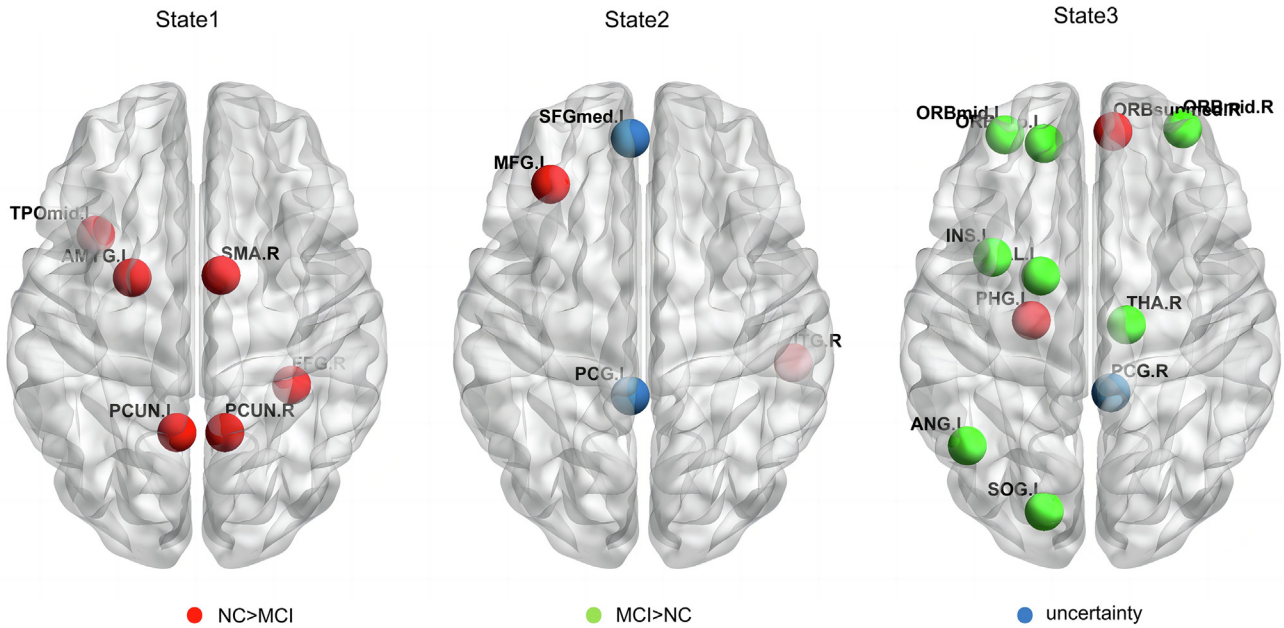


Fig. 8. Overlapping nodes with differences between MCI and NC groups. Red brain regions represent nodes that provide multiple functions in various communities of the NC group but not in the MCI group in both experiments. Green brain regions represent nodes that provide multiple functions in various communities of the MCI group but not in the NC group, while blue represents regions with opposite results in the two experiments.

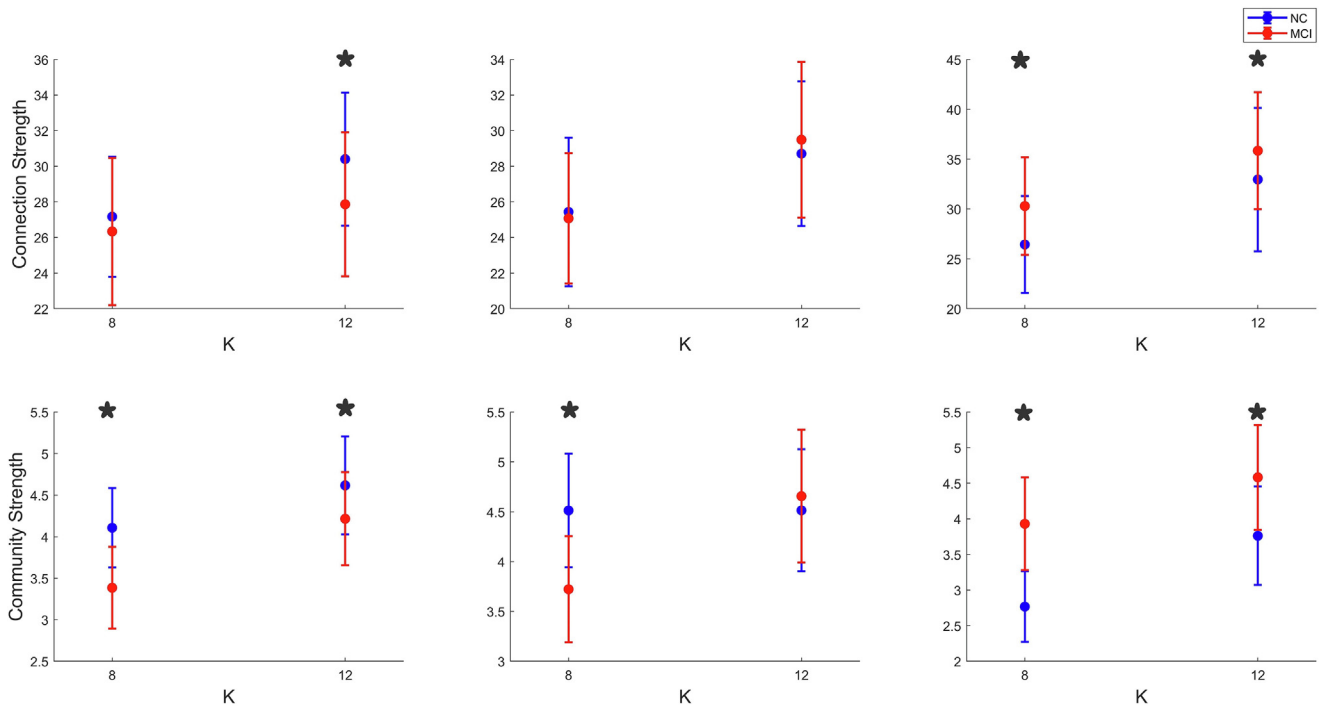


Fig. 9. Comparison of Functional Segmentation Indicators between MCI and NC Groups. The upper and lower rows depict the comparison of within-community connectivity strength and overall community strength for the three states in the NC group and MCI group, respectively, with $K = 8, 12$. The average values and standard deviations of both strengths for all participants are plotted, with asterisks denoting significant differences between the two groups ($p < 0.05$, t-tests, the absolute value of t is between 2.59 and 7.88).

community strength for each state in the two groups (see Fig. 9).

In state 1, both the within-community connectivity strength and overall community strength are stronger in

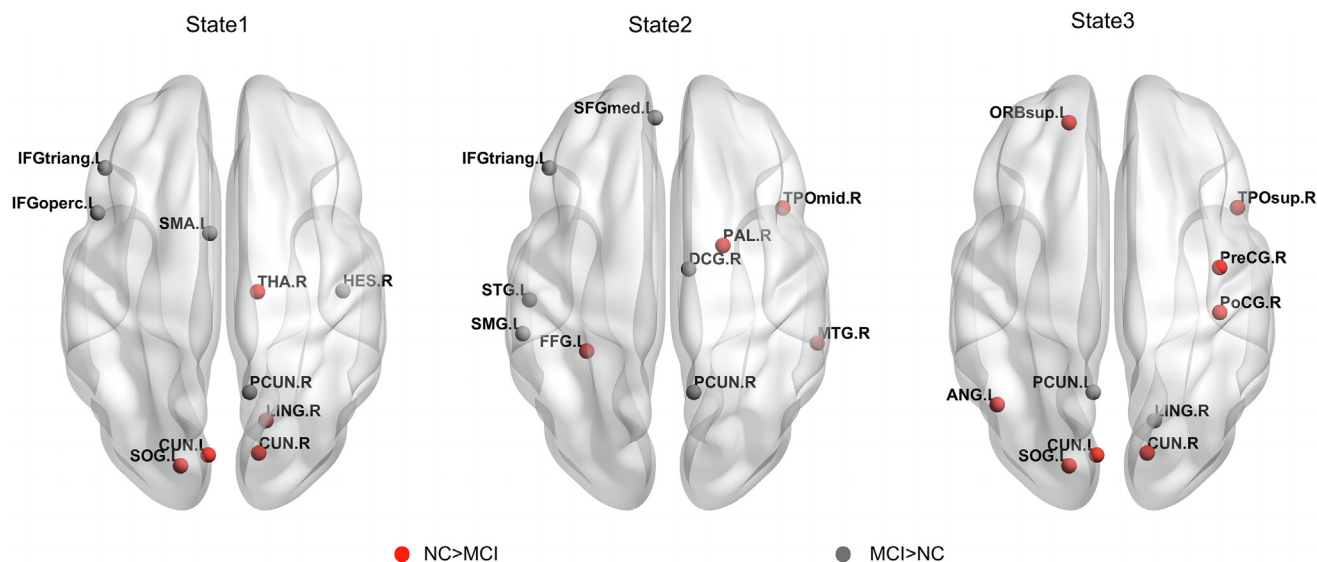


Fig. 10. Comparison of node functional diversity between MCI and NC Groups. The figure displays the top 10 nodes with the biggest mean differences in functional diversity that exhibited significance differences in both $k = 8$ and $k = 12$ conditions.

the NC group than the MCI group. In state 2, the differences in within-community connectivity strength and overall community strength between the NC and MCI groups are relatively small. In state 3, the within-community connectivity strength and overall community strength are generally lower in the NC group compared to the MCI group.

Node functional diversity. We separately calculated the functional diversity of nodes in the NC and MCI groups, followed by conducting significance difference tests ($p < 0.05$, t-tests). For each state, we selected the top 10 nodes with the biggest differences in functional diversity. The absolute values of the t-values obtained in state 1 for these brain regions range from 23.64 to 46.26, from 16.03 to 26.52 in state 2, and from 10.09 to 12.86 in state 3 (see Fig. 10).

Among them, IFGtriang.L (belonging to Attention), CUN.L, CUN.R, LING.R, SOG.L (belonging to Visual), and PCUN.R (belonging to Default mode) appeared repeatedly. Additionally, when comparing the MCI group to the NC group, functional diversity decreased in CUN.L, CUN.R, and SOG.L, but increased in IFGtriang.L and PCUN.R; LING.R exhibited decreased functional diversity in state 1 but increased in state 3.

DISCUSSION

This study investigated the differences in community detection of DFC patterns in MCI patients. Using k-means clustering on the functional connectivity matrices obtained from 2DPCA-reduced data, we explored various DFC patterns among participants. The CSSNMF method was applied for community detection of these patterns, enabling us to compare the community-specific within-module connectivity and overall community strength between MCI patients and the NC group.

Additionally, we computed node diversity metrics for both groups to identify nodes with significant differences.

Our findings reveal that within the clustering results, state 1 and state 2 are highly prevalent in both groups of participants, while state 3 is less common. Specifically, state 2, which accounts for 47.85% in the MCI group and 42.90% in the control group, exhibits a high degree of similarity. There are no significant differences in terms of optimal community numbers and functional segregation within this state. Notably, the disparities in the outcomes of community detection are mostly observed in nodes with lower community weights. In state 1, it constitutes 34.76% in the MCI group and 46.04% in the control group. There was a difference in the optimal number of communities between the two groups of participants. The differences in nodes are relatively limited, and in terms of functional segregation metrics, MCI patients exhibit lower community internal connection strength and overall community strength compared to the control group. Interestingly, in the less prevalent state 3, there are variations in optimal community numbers and substantial differences in community structures. In contrast to state 1, MCI patients in state 3 demonstrate higher community internal connection strength and overall community strength than the control group.

In both state 1 and state 3, the optimal community sizes of MCI patients were smaller than those of the NC group. This finding is consistent with a magnetoencephalography study on Alzheimer's Disease (AD). This research reveals a significant reduction in the number of brain modules in the AD group across different frequency bands (de Haan et al., 2012).

The decrease in the number of optimal communities may indicate that in the same states, the brain functional networks of MCI undergo certain changes, possibly due to a functional weakening in certain brain

regions, leading to compensatory shifts in other brain regions to fulfill the related functions (Han et al., 2022).

Comparing the experiments with community quantities set at 8 and 12, state 2 exhibited minor differences in community detection results between the two groups, mainly in nodes with lower community weights. There were no significant differences in within-module connectivity and overall community strength, which indicated that the resting-state brain activities in state 2 showed no substantial differences between MCI patients and the NC group. However, in states 1 and 3, significant differences were observed in community detection results, within-module connectivity, and overall community strength, aligning with our expectations. Interestingly, the direction of differences in within-module connectivity and overall community strength was reversed between these two states. In state 1, decreased within-module connectivity and overall community strength in MCI patients suggested a more dispersed and segregated brain functional network, indicating a weakened capacity of joint function across brain regions. In state 3, the opposite trend indicated that, compared to the NC group, MCI patients exhibited a more integrated and unified brain functional network in certain conditions. A similar phenomenon was also found in an EEG study of MCI, where cognitive tasks induced significantly higher increments of global network integration in MCI patients. MCI patients require more communication and recruitment across brain areas to maintain or improve task performance (Požar et al., 2023).

The opposite result of state 1 and state 3 may be due to the need for stronger global network integration for MCI patients to achieve certain functions in state 3, but not in state 1. This may be attributed to the different adaptive strategies adopted by the MCI brain in response to different states, which may be formed by different mechanisms and influencing factors (Bansal et al., 2019).

We further compared the differences among various brain regions within each community in the three states and identified nodes with significant differences that were consistently present in both experiments. We found differences in certain brain regions in state 1, including the Frontal Lobe, Parietal Lobe, Medial Temporal Lobe, Basal Ganglia, and Temporal Lobe. In state 2, differences were observed in the Frontal Lobe, Parietal Lobe, Occipital Lobe, and Temporal Pole. In state 3, differences were observed in the Frontal Lobe, Parietal Lobe, and Occipital Lobe.

The changes in these regions have been reported in previous research (Garcia-Alvarez et al. 2019; Bangen et al., 2020; Dadar et al., 2022; Yeung et al., 2022). Among the community difference nodes in the three states, only MFG.L, ORBinf.R, and STG.R repeatedly appeared. Perhaps in different states, MCI patients have different brain regions required for communication and recruitment to achieve corresponding functions (Bansal et al., 2019; Požar et al., 2023).

Furthermore, an analysis of node diversity differences revealed nodes with substantial mean differences in

functional diversity between $k = 8$ and $k = 12$. Among them, IFGtriang.L (Attention), CUN.L, CUN.R, LING.R, SOG.L (Visual), and PCUN.R (Default mode) were recurrent.

In the study on enhancing the feature representation of multi-modal MRI data for MCI classification (Liu et al., 2020), CUN.L, CUN.R, LING.R, SOG.L, and PCUN.R are important regions that repeatedly emerge in feature extraction across different modal data. These regions have also been reported in studies using the functional brain network estimation method for classification (Lei et al., 2020). Additionally, IFGtriang.L has been reported in research aiming to combine functional and structural information to obtain the most valuable features for diagnosing SCD and MCI (Lei et al., 2021).

A notable phenomenon was the fluctuation in LING.R's functional diversity between state 1 (decrease) and state 3 (increase). Maybe in state 3, MCI patients increased the connectivity of LING.R with other regions to achieve the corresponding function.

Several limitations of this study should be noted. First, the fMRI data collected were obtained using different scanner models, and the sample size was relatively small. The scanning duration for each participant was relatively short (9 minutes and 51 seconds). Secondly, determining appropriate functional connectivity states is a crucial issue. Lastly, the choice of community quantity was based on a conservative approach.

In summary, we found that there were differences in community structure between MCI and NC groups under different DFC states, including the optimal number of communities, functional separation, and Node Functional Diversity. Meanwhile, we identified some nodes with significant differences. We believe that research and findings conducted from this perspective can contribute to understanding of the neural network mechanisms of MCI.

This work is partly supported by the project of Jiangsu Key Research and Development Plan (BE2021012-2 and BE2021012-5), Changzhou Science and Technology Bureau Plan (CE20225034), Key Laboratory of Brain Machine Collaborative Intelligence Foundation of Zhejiang Province (2020E10010-04), and Human-Machine Intelligence and Interaction International Joint Laboratory Project. Data collection and sharing for this project was funded by the Alzheimer's Disease Neuroimaging Initiative (ADNI) National Institutes of Health Grant U01 AG024904.

Author contributions.

All authors have read and approved the manuscript. Hongwei Wang and Ling Zou organized, designed, and wrote the article. Hongwei Wang, Zhihao zhu, Hui Bia and Zhongyi Jiang conducted the experiment and analyzed the data. Yin Cao provided numerous improvement suggestions for the revision of the manuscript, offering valuable insights into the writing style and language. Suhong Wang and Ling Zou contributed to the preparation of the project, and have read and approved the final manuscript.

DECLARATION OF COMPETING INTEREST

The authors declare that they have no known competing financial interests or personal relationships that could have appeared to influence the work reported in this paper.

REFERENCES

- Allen EA, Damaraju E, Plis SM, Erhardt EB, Eichele T, Calhoun VD (2014) Tracking whole-brain connectivity dynamics in the resting state. *Cereb Cortex* 24:663–676.
- Bangen KJ, Thomas KR, Weigand AJ, Sanchez DL, Delano-Wood L, et al. (2020) Pattern of regional white matter hyperintensity volume in mild cognitive impairment subtypes and associations with decline in daily functioning. *Neurobiol Aging* 86:134–142.
- Bansal K, Garcia JO, Tompson SH, Verstynen T, Vettel JM, Muldoon SF (2019) Cognitive chimera states in human brain networks. *Sci Adv* 5 eaau8535.
- Chao-Gan Y, Yu-Feng Z (2010) DPARSF: a MATLAB Toolbox for “Pipeline” data analysis of resting-state fMRI. *Front Syst Neurosci* 4:13.
- Chen N, Shi J, Li Y, Ji S, Zou Y, et al. (2021) Decreased dynamism of overlapping brain sub-networks in Major Depressive Disorder. *J Psychiatr Res* 133:197–204.
- Chen P, Chen G, Zhong S, Chen F, Ye T, et al. (2022) Thyroid hormones disturbances, cognitive deficits and abnormal dynamic functional connectivity variability of the amygdala in unmedicated bipolar disorder. *J Psychiatr Res* 150:282–291.
- Dadar M, Manera AL, Ducharme S, Collins DL (2022) White matter hyperintensities are associated with grey matter atrophy and cognitive decline in Alzheimer’s disease and frontotemporal dementia. *Neurobiol Aging* 111:54–63.
- de Haan W, van der Flier WM, Koene T, Smits LL, Scheltens P, Stam CJ (2012) Disrupted modular brain dynamics reflect cognitive dysfunction in Alzheimer’s disease. *Neuroimage* 59:3085–3093.
- Du M, Zhang L, Li L, Ji E, Han X, et al. (2021) Abnormal transitions of dynamic functional connectivity states in bipolar disorder: a whole-brain resting-state fMRI study. *J Affect Disord* 289:7–15.
- Fathi S, Ahmadi M, Dehnad A (2022) Early diagnosis of Alzheimer’s disease based on deep learning: a systematic review. *Comput Biol Med* 146 105634.
- Gao Y, Sun J, Cheng L, Yang Q, Li J, et al. (2022) Altered resting state dynamic functional connectivity of amygdala subregions in patients with autism spectrum disorder: a multi-site fMRI study. *J Affect Disord* 312:69–77.
- Garcia-Alvarez L, Gomar JJ, Sousa A, Garcia-Portilla MP, Goldberg TE (2019) Breadth and depth of working memory and executive function compromises in mild cognitive impairment and their relationships to frontal lobe morphometry and functional competence. *Alzheimer’s Dementia: Diag Assess Dis Monitor* 11:170–219.
- Han H, Li X, Gan JQ, Yu H, Wang H, Alzheimer’s Disease Neuroimaging I (2022) Biomarkers derived from alterations in overlapping community structure of resting-state brain functional networks for detecting Alzheimer’s disease. *Neuroscience* 484:38–52.
- He Y, Wang J, Wang L, Chen ZJ, Yan C, et al. (2009) Uncovering intrinsic modular organization of spontaneous brain activity in humans. *PLoS One* 4 e5226.
- Hindriks R, Adhikari MH, Murayama Y, Ganzetti M, Mantini D, et al. (2016) Can sliding-window correlations reveal dynamic functional connectivity in resting-state fMRI? *Neuroimage* 127:242–256.
- Jiao Z, Gao P, Ji Y, Shi H (2021) Integration and segregation of dynamic functional connectivity states for mild cognitive impairment revealed by graph theory indicators. *Contrast Media Mol Imaging* 2021 6890024.
- Lei B, Cheng N, Frangi AF, Tan E-L, Cao J, et al. (2020) Self-calibrated brain network estimation and joint non-convex multi-task learning for identification of early Alzheimer’s disease. *Med Image Anal* 61.
- Lei B, Cheng N, Frangi AF, Wei Y, Yu B, et al. (2021) Auto-weighted centralised multi-task learning via integrating functional and structural connectivity for subjective cognitive decline diagnosis. *Med Image Anal* 74.
- Li X, Gan JQ, Wang H (2018) Collective sparse symmetric non-negative matrix factorization for identifying overlapping communities in resting-state brain functional networks. *Neuroimage* 166:259–275.
- Liu C, Zhao L, Xu K, Wei Y, Mai W, et al. (2022) Altered functional connectivity density in mild cognitive impairment with moxibustion treatment: a resting-state fMRI study. *Brain Res* 1775 147732.
- Liu J, Pan Y, Wu F-X, Wang J (2020) Enhancing the feature representation of multi-modal MRI data by combining multi-view information for MCI classification. *Neurocomputing* 400:322–332.
- Ma ZZ, Wu JJ, Hua XY, Zheng MX, Xing XX, et al. (2021) Tracking whole-brain connectivity dynamics in the resting-state fMRI with post-facial paralysis synkinesis. *Brain Res Bull* 173:108–115.
- Najafi M, McMenamin BW, Simon JZ, Pessoa L (2016) Overlapping communities reveal rich structure in large-scale brain networks during rest and task conditions. *Neuroimage* 135:92–106.
- Požar R, Kero K, Martin T, Giordani B, Kavcic V (2023) Task aftereffect reorganization of resting state functional brain networks in healthy aging and mild cognitive impairment. *Front Aging Neurosci* 14.
- Prieto del Val L, Cantero JL, Baena D, Atienza M (2018) Damage of the temporal lobe and APOE status determine neural compensation in mild cognitive impairment. *Cortex* 101:136–153.
- Spencer APC, Goodfellow M (2022) Using deep clustering to improve fMRI dynamic functional connectivity analysis. *Neuroimage* 257 119288.
- van den Heuvel MP, Hulshoff Pol HE (2010) Exploring the brain network: a review on resting-state fMRI functional connectivity. *Eur Neuropsychopharmacol* 20:519–534.
- Vataman A, Ciolac D, Chiosa V, Aftene D, Leahu P, et al. (2023) Dynamic flexibility and controllability of network communities in juvenile myoclonic epilepsy. *Neurobiol Dis* 179 106055.
- Wang Z, Jia X, Liang P, Qi Z, Yang Y, et al. (2012) Changes in thalamus connectivity in mild cognitive impairment: evidence from resting state fMRI. *Eur J Radiol* 81:277–285.
- Wei L, Zhang Y, Wang J, Xu L, Yang K, et al. (2022) Parietal-hippocampal rTMS improves cognitive function in Alzheimer’s disease and increases dynamic functional connectivity of default mode network. *Psychiatry Res* 315.
- Xu F, Qiao C, Zhou H, Calhoun VD, Stephen JM, et al. (2023) An explainable autoencoder with multi-paradigm fMRI fusion for identifying differences in dynamic functional connectivity during brain development. *Neural Netw* 159:185–197.
- Yeung MK, Chau AK-Y, Chiu JY-C, Shek JT-L, Leung JP-Y, Wong TC-H (2022) Differential and subtype-specific neuroimaging abnormalities in amnesic and nonamnesic mild cognitive impairment: a systematic review and meta-analysis. *Ageing Res Rev* 80.
- Zhang L, Fu Z, Zhang W, Huang G, Liang Z, et al. (2021) Accessing dynamic functional connectivity using l0-regularized sparse-smooth inverse covariance estimation from fMRI. *Neurocomputing* 443:147–161.
- Zhu Z, Wang H, Bi H, Lv J, Zhang X, et al. (2023) Dynamic functional connectivity changes of resting-state brain network in attention-deficit/hyperactivity disorder. *Behav Brain Res* 437 114121.
- Zhuang X, Yang Z, Mishra V, Sreenivasan K, Bernick C, Cordes D (2020) Single-scale time-dependent window-sizes in sliding-window dynamic functional connectivity analysis: A validation study. *Neuroimage* 220 117111.